

1 **Tropospheric warming over the North Indian Ocean caused by the South Asian**
2 **anthropogenic aerosols: possible impact on the upper troposphere and lower**
3 **stratosphere**

4
5 Suvarna Fadnavis^{1*}, Prashant Chavan¹, Akash Joshi², Sunil Sonbawne¹, Asutosh Acharya³,
6 Panuganti C S. Devara⁴, Alexandru Rap⁵, Felix Ploeger⁶ and Rolf Müller⁶

7 ¹Indian Institute of Tropical meteorology, MoES, Pune, India

8 ²Indian Institute of Technology, Kharagpur, India

9 ³Indian Institute of Technology, Bhubneshwar, India

10 ⁴Centre of Excellence in ACOAST/ACESH, Amity University Haryana (AUH), Gurugram
11 122413, India

12 ⁵School of Earth and Environment, University of Leeds, Leeds, United Kingdom

13 ⁶Forschungszentrum Jülich GmbH, IEK-7, Jülich, Germany

14 Corresponding author: Suvarna Fadnavis

15 Corresponding author email: suvarna@tropmet.res.in

16
17
18 **Abstract**

19 Atmospheric concentrations of South Asian anthropogenic aerosols and their transport play a
20 key role in the regional hydrological cycle. Here, we use the ECHAM6-HAMMOZ
21 chemistry-climate model to show the structure and implications of the transport pathways of
22 these aerosols during spring (March-May). Our simulations indicate that large amounts of
23 anthropogenic aerosols are transported from South Asia to the North Indian Ocean and
24 Western Pacific. These aerosols are then lifted into the upper troposphere and lower
25 stratosphere (UTLS) by the ascending branch of the Hadley circulation, where they enter the
26 westerly jet. They are further transported to the Southern Hemisphere (~15° S – 30° S), and
27 downward (320 – 340K) via westerly ducts over the tropical Atlantic (5° S – 5° N, 10° W – 40°
28 W) and Pacific (5° S – 5° N, 95° E – 140° E). The carbonaceous aerosols are also transported to
29 the Arctic leading to local heating (0.08 – 0.3 K month⁻¹, an increase by 10 – 60 %).

30 The presence of anthropogenic aerosols causes a negative radiative forcing (RF) at the TOA
31 $(-0.90 \pm 0.089 \text{ W m}^{-2})$ and surface $(-5.87 \pm 0.31 \text{ W m}^{-2})$ and atmospheric warming $(+4.96 \pm 0.24$
32 $\text{W m}^{-2})$ over South Asia ($60^\circ \text{ E} - 90^\circ \text{ E}$, $8^\circ \text{ N} - 23^\circ \text{ N}$), except over the Indo-Gangetic plain
33 ($75^\circ \text{ E} - 83^\circ \text{ E}$, $23^\circ \text{ N} - 30^\circ \text{ N}$) where RF at the TOA is positive $(+1.27 \pm 0.16 \text{ W m}^{-2})$ due to
34 large concentrations of absorbing aerosols. The carbonaceous aerosols lead to in-atmospheric
35 heating along the aerosol column extending from the boundary layer to the upper troposphere
36 $(0.1 \text{ to } 0.4 \text{ K month}^{-1}$, increase by 4 – 60 %) and in the lower stratosphere $40^\circ \text{ S} - 90^\circ \text{ N}$ $(0.02$
37 $\text{to } 0.3 \text{ K month}^{-1}$, increase by 10 – 60 %). The increase in tropospheric heating due to aerosols
38 results in an increase in water vapor concentrations, which are then transported from the
39 North Indian Ocean-Western Pacific to the UTLS over $45^\circ \text{ S} - 45^\circ \text{ N}$ (increasing water vapor
40 by 1 - 10 %).

41 Keywords: South Asian Anthropogenic aerosols; warming over the Arabian Sea; transport of
42 aerosols and water vapor to the UTLS in spring.

43 1. Introduction

44 Understanding the variability of anthropogenic aerosol loading over the North Indian
45 Ocean is of utmost importance since (1) it regulates the Asian hydrological cycle via
46 modulating atmospheric convection, heating rates, and moisture transport (Ramanathan et al.,
47 2005; Corrigan et al., 2008; Budhavant et al., 2018, Meehl et al., 2008), and (2) it leads to
48 adverse impacts on marine ecosystems (Mahowald et al., 2018; Collins et al., 2019). Several
49 observations indicate that the aerosol loading over the North Indian Ocean during the spring
50 season is strongly influenced by South Asian aerosols. Aircraft measurements during the
51 Indian Ocean Experiment (INDOEX) (February–March 1999) showed the presence of a thick
52 layer (surface to 3.2 km) of anthropogenic aerosols (BC~14 %, sulfate 34 %, ammonium 11
53 %) over the North Indian Ocean (Dickerson et al., 2002; Mayol-Bracero et al., 2002) with
54 sources over South Asia. [Several other in situ observations, e.g. over the Maldives during
55 November 2014 – March 2015, show that air masses arising from the Indo-Gangetic Plain
56 contain very high amounts \(97 %\) of the elemental carbon in the PM₁₀ in the fine mode.](#)
57 (Bhuhvant et al., 2018). Observations from the Geosphere-Biosphere Programme over the
58 Bay of Bengal during spring (March 2016) also show abundant anthropogenic aerosols
59 (sulfate and nitrate) having sources over the Indo-Gangetic plain (Nair et al., 2017).

60 The aerosol loading over South Asia has been increasing at an alarming rate (rate of
61 increase in AOD 0.004 per year during 1988 – 2013) (Babu et al., 2013). For the last two
62 decades, the AOD increase (by 12 %) over [South](#) Asia has been attributed to the strong
63 increase in anthropogenic aerosols (sulfate, black carbon, and organic carbon), while natural
64 aerosol remained unchanged (Ramachandran et al., 2020a). The major sources of
65 anthropogenic aerosols are the combustion of domestic fuels, industrial emissions,
66 transportation, and open burning (Paliwal et al., 2016). The growth of the economy of India

67 led to a 41 % increase in BC and 35 % in OC from 2000 to 2010 (Lu et al., 2011). The
68 emissions of sulfur dioxide (SO₂) which leads to the production of sulfate aerosols have
69 doubled during 2006 – 2017 (Fadnavis et al., 2019). Figure 1 a-c shows the annual mean
70 emission of BC, OC, and sulfate aerosols over South Asia in 2016 from AEROCOM-
71 ACCMIP-II emission inventory (discussed in section 2.1). It shows high emissions over the
72 Indo-Gangetic Plain (BC 7×10^{-12} – 17×10^{-12} Kg m⁻² S⁻¹, OC: 25×10^{-12} - 70×10^{-12} Kg m⁻² S⁻¹,
73 sulfate: 2×10^{-12} - 5×10^{-12} Kg m⁻² S⁻¹). Higher amounts of aerosols over the Indo-Gangetic
74 Plain are associated with densely populated regions and industrial and vehicular emissions
75 (Karambelas et al., 2018, Fadnavis et al., 2019). Past studies also show substantially higher
76 amounts of aerosols over North India compared to the rest of the Indian region
77 (Ramachandran et al., 2020b, Fadnavis et al., 2013, 2017a, 2017b). Over the Indo-Gangetic
78 plain, these emissions show a peak in spring (Fig. 1d), with increases for BC of 0 – 3 %, OC
79 0 – 8.7 %, and sulfate 0 – 0.2 %, compared to annual means. This peak in emissions in spring
80 is to a large extent driven by springtime agricultural crop burning and biomass burning
81 activity (Chavan et al., 2021).

82 While the presence of sulfate aerosols leads to a cooling of the atmosphere below due to
83 their strong scattering properties, carbonaceous aerosols produce atmospheric warming via
84 absorption of solar radiation (Fadnavis et al., 2019, Penner et al., 1998). Previous studies
85 showed that the doubling of carbonaceous aerosols loading over South Asia (10° S – 50° N,
86 65° E – 155° E) led to significant atmospheric warming (in-atmospheric RF 5.11W m⁻²,
87 Fadnavis et al. 2017b).

88

89

90

91

92

93

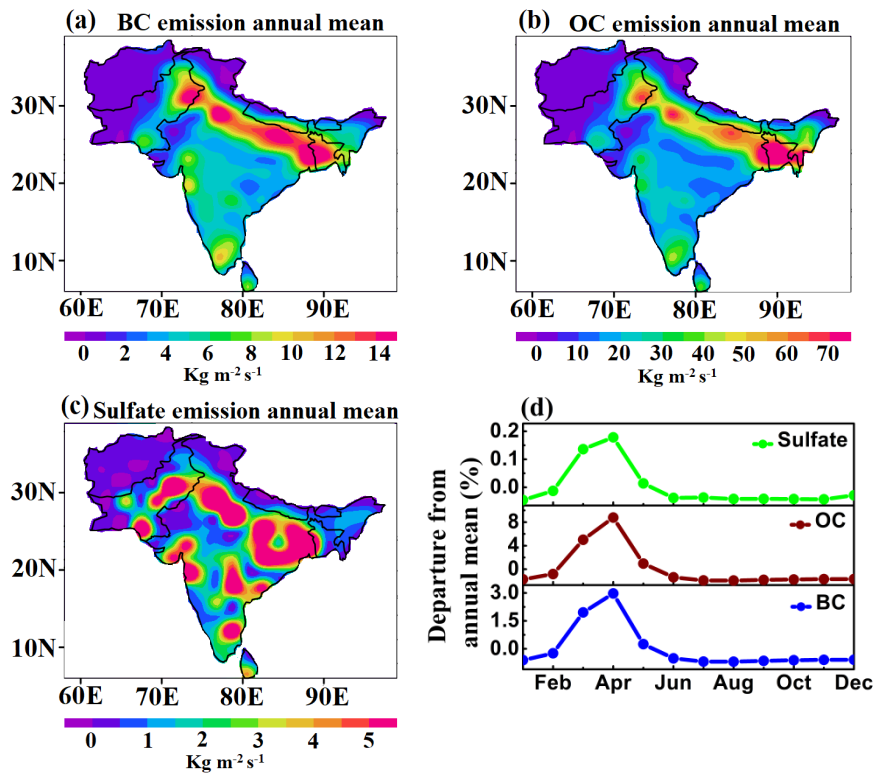
94

95

96

97

98



99 Figure 1: Spatial distribution for the year 2016 annual mean total emission ($\text{kg m}^{-2} \text{S}^{-1}$) of
100 (a) BC, (b) OC, (c) Sulfate aerosols from AEROCOM-ACCMIP-II emission inventory, (d)
101 time series of monthly departure from annual mean total emissions (%) of BC, OC, and
102 Sulfate aerosols averaged over Indo-Gangetic plain ($23^\circ \text{N} - 30^\circ \text{N}$, $78^\circ \text{E} - 90^\circ \text{E}$).

103 During spring, the prevailing convective instability over the Bay of Bengal and the
104 Arabian Sea transports aerosol from the boundary layer to the upper troposphere
105 (Romatschke and Houze, 2011). Airborne observations during winter and spring, e.g. the
106 Civil Aircraft for Regular Investigation of the Atmosphere based on an Instrument Container
107 (CARIBIC) in March 1999 and January 2001 (Papasiropoulos et al., 2002), and the Indian
108 Ocean Experiment (INDOEX) in February-March 1999 show elevated aerosol amounts near
109 8 – 12 km over the Indian Ocean and South Asia (De Reus et al., 2001). Recently, using a set
110 of model simulations, Chavan et al., (2021) reported the transport of biomass burning
111 aerosols to the upper troposphere by convection in spring 2013.

112 Here, we investigate the source of the very large aerosol loading over the Arabian Sea
113 during spring and, their [vertical transport to the UTLS](#). We show these aerosols produce
114 atmospheric warming leading to enhanced water vapor that is transported to the UTLS. Once
115 in the lower stratosphere, [aerosols and water vapour are transported to the Southern](#)
116 [hemisphere](#) (~45° S), with implications on tropospheric temperatures and stratospheric ozone
117 concentrations. For this purpose, we performed a series of five simulations using the
118 ECHAM6-HAMMOZ model in order to investigate the impact of changes in anthropogenic
119 aerosol over South Asia. [The paper is structured as follows: the ECHAM6-HAMMOZ model](#)
120 [simulations are provided in section 2, in section 3 we discuss the results on the transport of](#)
121 [South Asian aerosols to the North Indian Ocean, radiative forcing, transport into the UTLS,](#)
122 [and associated impacts on heating rates, while conclusions are summarised in section 4.](#)

123 **2. Model simulations**

124 **2.1 ECHAM6-HAMMOZ experimental set-up**

125 We use the state of [the art aerosol–chemistry–climate model](#) ECHAM6–HAMMOZ. It
126 comprises of the general circulation module ECHAM6, coupled to the aerosol and cloud
127 microphysics module [Hamburg](#) (HAM) (Stier et al., 2005; Tegen et al., 2019). HAM
128 predicts the nucleation, growth, evolution, and sinks of sulfate, black carbon (BC), [organic](#)
129 [carbon \(OC\)](#), sea salt (SS), and mineral dust (DU) aerosols. The size distribution of the
130 aerosol population is described by seven log-normal modes ([Nucleation mode, soluble and](#)
131 [insoluble Aitken, soluble and insoluble accumulation and soluble and insoluble coarse](#)
132 [modes](#)) (Stier et al., 2005; Zhang et al., 2012; Tegen et al., 2019). Moreover, HAM
133 explicitly simulates the impact of aerosol species on cloud droplet and ice crystal formation
134 [according to prescribed microphysical properties. Aerosol particles can act as cloud](#)
135 [condensation nuclei or as kernel for ice-nucleating particles.](#) Other relevant cloud

136 microphysical processes such as evaporation of cloud droplets, sublimation of ice crystals,
137 ice crystal sedimentation, and detrainment of ice crystals from convective cloud tops are
138 simulated interactively (Neubauer et al., 2014). The anthropogenic and fire emissions of
139 sulfate, black carbon (BC), and organic carbon (OC) are based on the AEROCOM-
140 ACCMIP-II emission inventory. Other details of the model and emissions are reported by
141 Fadnavis et al. (2017a, 2019, 2021a, b).

142 The model simulations are performed at a T63 spectral resolution corresponding to
143 $1.875^\circ \times 1.875^\circ$ in the horizontal dimension, while the vertical resolution is described by 47
144 hybrid σ -p levels from the surface up to 0.01 hPa (approx. 80 km). The simulations have
145 been carried out with a time step of 20 min. Monthly varying Atmospheric Model Inter-
146 comparison Project (AMIP) sea surface temperature (SST) and sea ice cover (SIC) (Taylor et
147 al., 2000) were used as lower boundary conditions.

148 We performed five model experiments: (1) a control (CTL) simulation where all aerosol
149 emissions are included and four perturbed experiments where (2) all anthropogenic aerosol
150 emissions (black carbon, organic carbon, and sulfate) are switched off over South Asia (75° E
151 $- 100^\circ$ E, 8° N $- 40^\circ$ N, see Fig. 1) during the study period (2001 $-$ 2016) (referred to as
152 Aerooff), (3) only anthropogenic black carbon emissions (BC) switched off during the study
153 period, (BCoff), (4) only anthropogenic organic carbon (OC) emissions switched off (OCoff)
154 during the study period, and (5) only anthropogenic sulfate aerosol emissions switched off
155 (Suloff) during the study period (see Table 1). All simulations were performed from 1
156 January 2001 to December 2016 from stabilized initial fields created after a model integration
157 for one year. Dust emission parameterization is the same in all the simulations and is based
158 on Tegen et al. (2002). The analysis is performed for spring (March $-$ May) averaged for the
159 period 2001 $-$ 2016. We compare the CTL with Aerooff, BCoff, OCOff, and Suloff
160 simulations to understand (1) transport path ways of South Asian anthropogenic aerosols, and

161 (2) their impact over the Indian region, and UTLS (340K – 400K). We compare AOD from
 162 CTL simulations with MISR and MODIS data (section S1). The model performance against
 163 MISR and MODIS (Kahn et al., 2007) for the spring season is discussed in section S2 from
 164 Fig. S1. We use the 2 PV contour in mid-latitudes and the 380 K isentrope in the tropics as an
 165 estimate of the location of the dynamical tropopause (Holton et al., 1995). Note that the PV
 166 value at the dynamical tropopause is often somewhat higher than 2 PV and exhibits a certain
 167 variability (Kunz et al., 2011).

168 Table -1: Details of ECHAM6-HAMMOZ model simulations performed in this study.

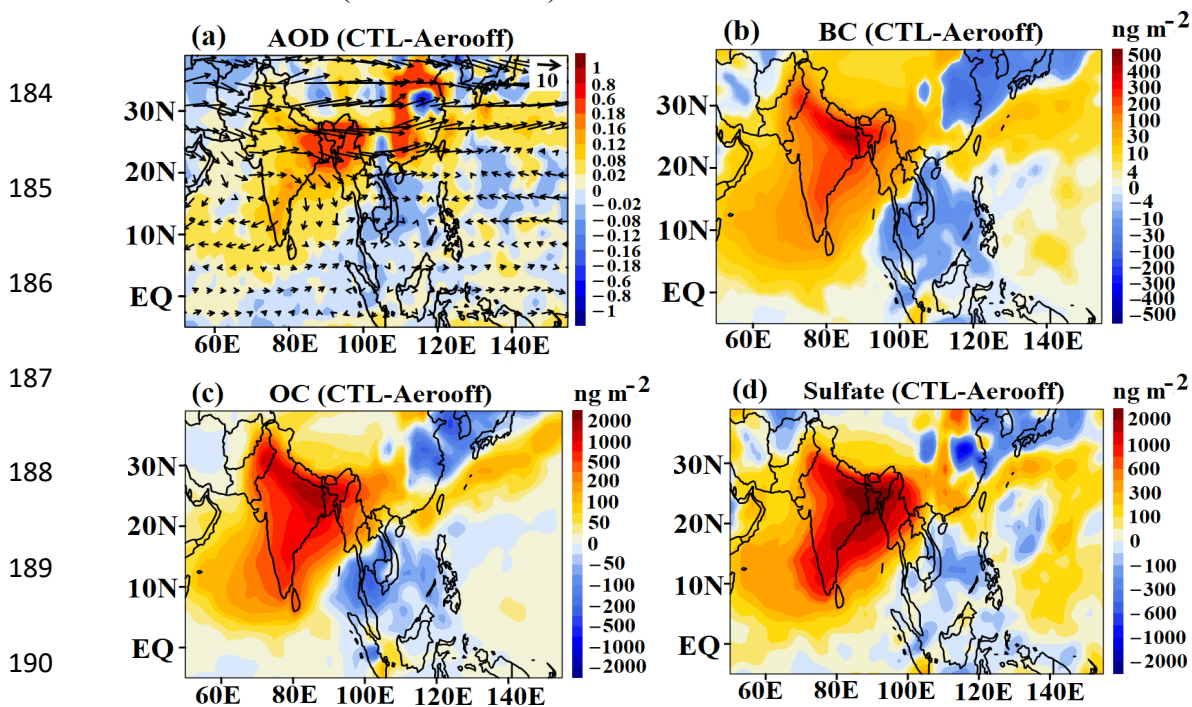
Experiment name	Duration	Aerosol species on/off	Boundary conditions
CTL	2001 – 2016	All aerosols species globally, as per AEROCOM-ACCMIP-II emission inventory.	AMIP Sea surface temperature and sea ice concentration.
Aerooff	2001 – 2016	Anthropogenic BC, OC, and sulfate aerosols switch off over South Asia during 2001 – 2016.	AMIP Sea surface temperature and sea ice concentration.
BCoff	2001 – 2016	Anthropogenic BC aerosols switch off over South Asia during 2001 – 2016.	AMIP Sea surface temperature and sea ice concentration.
OCoff	2001 – 2016	Anthropogenic OC aerosols switch off over South Asia during 2001 – 2016.	AMIP Sea surface temperature and sea ice concentration.
Suloff	2001 – 2016	Anthropogenic sulfate aerosols switch off over South Asia during 2001 – 2016.	AMIP Sea surface temperature and sea ice concentration.

169 3. Results and discussions

170 3.1 Transport of South Asian aerosols to the North Indian Ocean

171 The spatial distribution of AOD anomalies from the CTL-Aerooff simulation shows
 172 positive anomalies of AOD extending from South Asia to the Arabian Sea and the North Bay

173 of Bengal (10° N - 20° N) (Fig. 2a). The wind vectors indicate that these are transported from
 174 the Indo-Gangetic plain to the Arabian Sea, the Bay of Bengal and Western Pacific. The
 175 transported aerosols enhanced the AOD by 0.18 - 0.8 (30 - 80 %) over the North Bay of
 176 Bengal and by 0.02 - 0.12 (20 - 60 %) over the Arabian Sea. This is consistent with previous
 177 studies where 50 - 60 % enhancements in the AOD over the tropical Indian Ocean due to
 178 anthropogenic aerosols have been reported (Satheesh et al. 2000; Jose et al. 2020). Chemical
 179 analysis of aerosols observed over the south-eastern coastal Arabian Sea also shows the
 180 dominance of anthropogenic aerosols having sources over the Indian region (73 %) (Aswini
 181 et al., 2020). Analysis of MODIS satellite observations (2003 - 2017) likewise shows that
 182 anthropogenic sources contributed ~60 - 70% to the aerosol loading over the east coast and
 183 west coast of India (Jose et al. 2020).



191 Figure 2: Spatial distribution of (a) AOD anomalies averaged for spring during 2001 -
 192 2016 (CTL - Aerooff), and anomalies of tropospheric column of (b) BC, (c) OC, and (d)
 193 sulfate aerosols (ng m⁻²) (CTL-Aerooff). The vectors in Fig.2a indicate winds (m s⁻¹) at
 194 850 hPa.

195 The distribution of anomalies of the tropospheric column of BC, OC, and sulfate aerosols
196 also indicates that these aerosols are transported from South Asia to the Bay of Bengal and
197 the Arabian Sea (Fig. 2b-d). Enhancement of sulfate and OC aerosol ($50 - 2000 \text{ ng m}^{-2}$) is
198 higher than BC ($4 - 500 \text{ ng m}^{-2}$) over the South Asian region (Fig. 2b-d). The total
199 carbonaceous aerosol (BC and OC together) dominates over the sulfate aerosols. These
200 anthropogenic aerosols over the tropical Indian Ocean affect the radiation budget and cloud
201 cover over the Indian Ocean (Satheesh et al., 2000; McFarquhar and Wang, 2006).

202 3.2. Radiative forcing

203 The anthropogenic aerosols over the tropical Indian Ocean affect the radiation budget and
204 cloud cover (McFarquhar and Wang, 2006). Here, we discuss the impact of South Asian
205 anthropogenic aerosols on RF. Figures 3a-c show anomalies in net RF at the TOA, surface,
206 and in-atmosphere (TOA - surface) for Aerooff simulations (CTL - Aerooff). The
207 anthropogenic aerosols have produced a cooling at the TOA (except over the Indo-Gangetic
208 plain) and at the surface (see Fig. 3a-b). The simulated RF values over the Arabian Sea (55°
209 $E - 70^\circ E$, $8^\circ N - 20^\circ N$), Bay of Bengal ($88^\circ E - 92^\circ E$, $12^\circ N - 20^\circ N$), and Indo-Gangetic
210 Plain ($75^\circ E - 83^\circ E$, $26^\circ N - 30^\circ N$) are tabulated in Table-S1. The RF estimates show that
211 the aerosols have produced cooling at the TOA and surface over the Arabian Sea (TOA: -
212 $0.72 \pm 0.14 \text{ W m}^{-2}$, surface: $-3.0 \pm 0.28 \text{ W m}^{-2}$), Bay of Bengal (TOA: $-1.24 \pm 0.15 \text{ W m}^{-2}$, surface:
213 $-5.14 \pm 0.44 \text{ W m}^{-2}$), and in-atmospheric warming over the above regions (Arabian Sea
214 $+2.27 \pm 0.19 \text{ W m}^{-2}$; Bay of Bengal: $+3.89 \pm 0.30 \text{ W m}^{-2}$) (Fig. 3 c). The Indo Gangetic Plain
215 shows positive anomalies of RF at the TOA ($+1.27 \pm 0.16 \text{ W m}^{-2}$), negative at the surface (-
216 $11.16 \pm 0.50 \text{ W m}^{-2}$), and an atmospheric warming of $+12.44 \pm 0.42 \text{ W m}^{-2}$. In agreement with
217 our results, previous studies have reported negative RF at the surface and TOA, and
218 atmospheric warming over the North Indian Ocean caused by enhanced anthropogenic
219 aerosol. For example, Pathak et al. (2020) reported negative aerosol RF at the TOA (-2 to -4

220 W m^{-2}) over the Bay of Bengal and the Arabian Sea during spring 2009 - 2013. The clear sky
221 aerosol direct radiative forcing estimated from measurements during the INDOEX
222 experiment (January to March in 1999) over the North Indian Ocean also show similar
223 results (TOA: -7 W m^{-2} , surface: -23 W m^{-2} , and in-atmosphere: $+16 \text{ W m}^{-2}$) (Ramanathan et
224 al., 2001). There is a large variation in the magnitude of RF (at the TOA, surface, and in-
225 atmosphere) reported from observations and our model simulations. This may be due to
226 different regions and different time periods and the relatively coarse model resolution. The
227 observation-based studies attribute positive in-atmospheric radiative forcing to absorbing
228 aerosols (especially black carbon) that lead to a heating of the atmosphere (Rajeev and
229 Ramanathan, 2001; Satheesh et al., 2002).

230 The analysis of the perturbed model experiments indicates that anthropogenic BC
231 aerosols (Fig. 3d-f) have produced a warming at the TOA (Arabian Sea: $1.24 \pm 0.13 \text{ W m}^{-2}$,
232 Bay of Bengal: $1.54 \pm 0.26 \text{ W m}^{-2}$, Indo-Gangetic Plain: $4.33 \pm 0.17 \text{ W m}^{-2}$) and cooling at the
233 surface (Arabian Sea: $-2.56 \pm 0.25 \text{ W m}^{-2}$, Bay of Bengal: $-3.70 \pm 0.49 \text{ W m}^{-2}$, Indo-Gangetic
234 Plain: $-9.27 \pm 0.37 \text{ W m}^{-2}$). OC (Fig. 3g-i) and sulfate (Fig. 3j-l) aerosols have produced
235 significant cooling at the TOA (OC: -0.21 ± 0.13 to $-0.44 \pm 0.15 \text{ W m}^{-2}$; Sulfate: -1.55 ± 0.16 to -
236 $2.14 \pm 0.17 \text{ W m}^{-2}$) and surface (OC: -0.49 ± 0.31 to $-2.56 \pm 0.45 \text{ W m}^{-2}$, Sulfate: -1.19 ± 0.24 to -
237 $2.67 \pm 0.36 \text{ W m}^{-2}$) over the above regions (listed in Table-S1). Figures 3d, 3g, and Fig. 3j
238 further confirm our finding that the positive anomalies of radiative forcing in the Indo-
239 Gangetic plain are due to BC aerosols because of its absorbing property. All the aerosols
240 produce in-atmospheric warming over the Indian region (Fig. 3c, 3f, 3i, 3l) and the North
241 Indian Ocean (Fig. 3c, 3f, 3i). The atmospheric warming over the Arabian Sea and Bay of
242 Bengal is due to BC and OC aerosols with larger contributions by the BC aerosols.

243

244

245

246

247

248

249

250

251

252

253

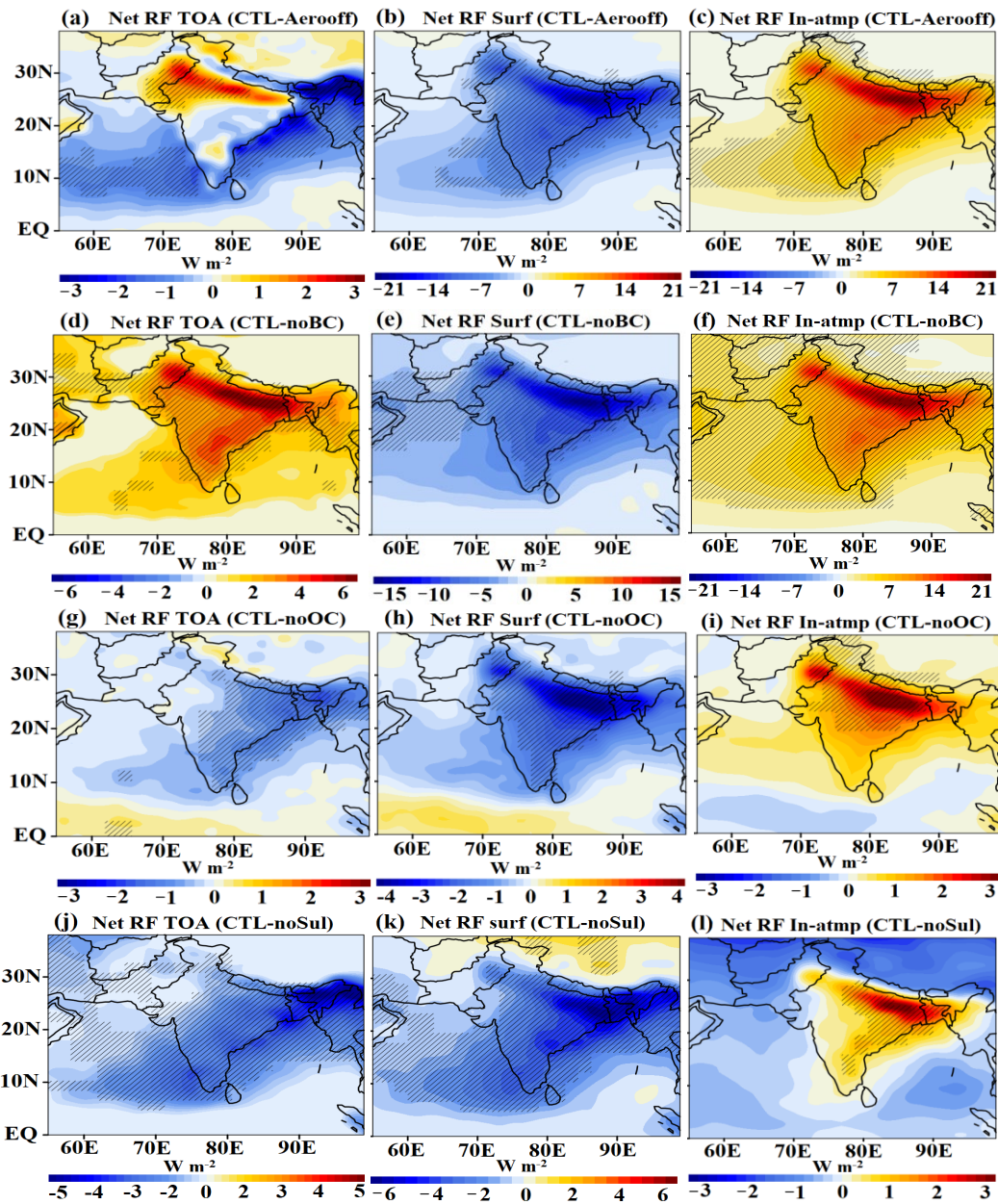
254

255

256

257

258



259 Figure 3: Spatial distribution of **net** aerosol radiative forcing (CTL - Aerooff) ($W m^{-2}$)
 260 averaged for spring **for the years** 2001 – 2016 (a) TOA, (b) same as (a) but for surface, (c)
 261 same as (a) but for in-atmosphere (TOA - surface), (d) spatial distribution of radiative
 262 forcing at the TOA (CTL – BCoff) averaged for spring **for the years** 2001 – 2016, (e) same
 263 as (d) but for surface, (f) same as (d) but for in-atmosphere (TOA - surface), (g) spatial
 264 distribution of radiative forcing at the TOA (CTL - OCoff) averaged for spring during
 265 2001 – 2016, (h) same as (g) but for surface, (i) same as (h) but for in-atmosphere (TOA -
 266 surface), (j) spatial distribution of radiative forcing at the TOA (CTL - Suloff) averaged
 267 for spring during 2001 – 2016, (k) same as (j) but for surface, (l) same as (k) but for in-
 268 atmosphere (TOA - surface). The hatched lines in figure a-l indicate 99% confidence level
 269 for the mean differences.

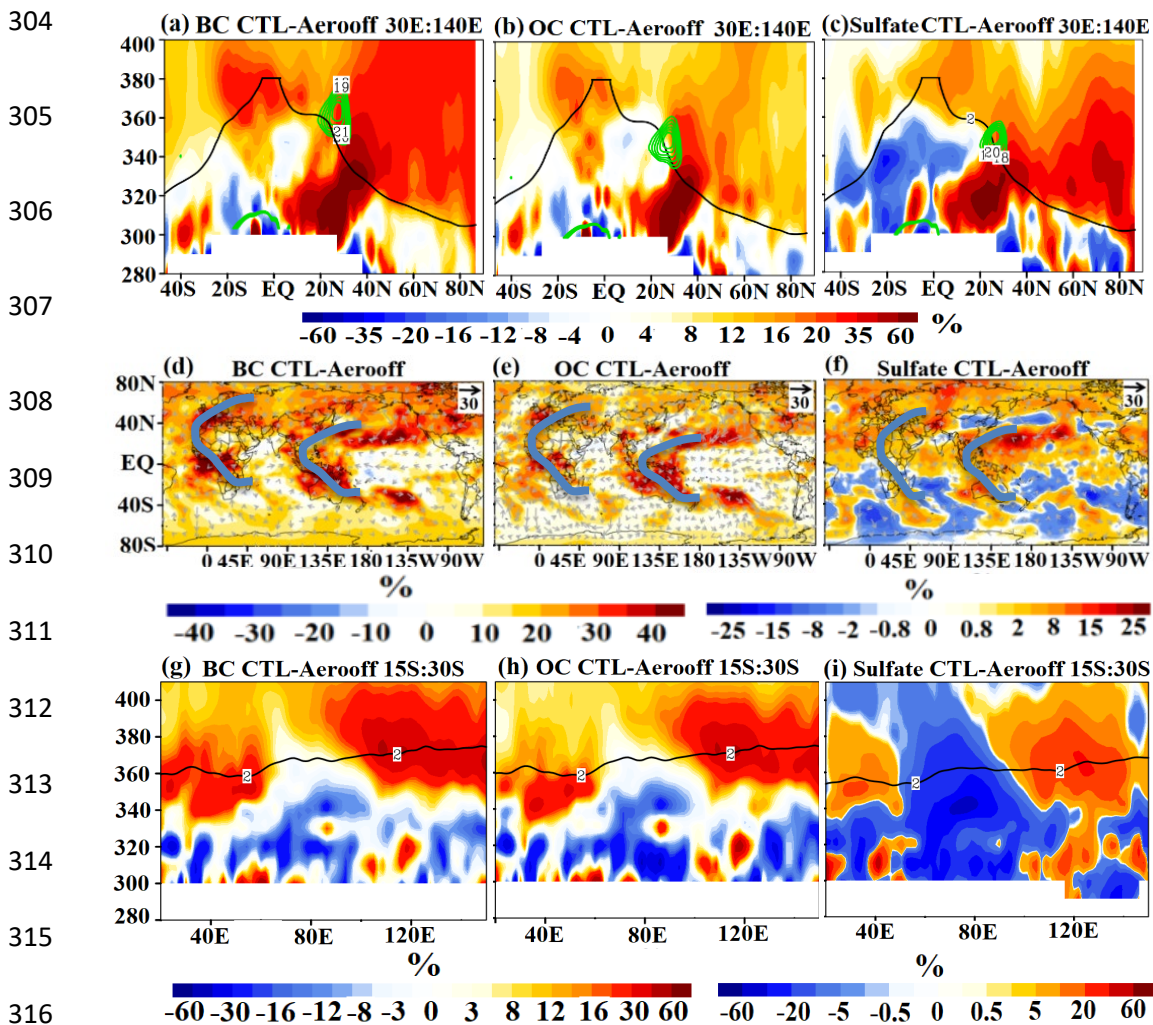
270 3.3. Transport of Asian anthropogenic aerosols into the UTLS

271 Further, we investigate the vertical distribution of aerosols that are transported to the
272 North Indian Ocean. This analysis is performed on the isentropic levels, since past studies
273 show that air mass transport from the troposphere to the stratosphere occurs largely along
274 quasi-isentropic surfaces (Ploeger et al., 2017; Yan et al., 2021). In spring, Asian aerosols are
275 transported partly to the Arabian Sea and Bay of Bengal region and partly to the Western
276 Pacific (Fig. 2a-d). Hence the meridional section is shown over the Indian Ocean and western
277 Pacific region (30° E – 140° E) (Fig. 4 a-c). The vertical distribution of BC, OC, and sulfate
278 aerosols indicates that these aerosols are transported from the boundary layer (10° N – 30° N)
279 into the UTLS (340 – 400K) (Fig. 4a-c and Fig. S2). In the UTLS, at ~ 350 K – 390 K they are
280 transported southward ($\sim 30^{\circ}$ S) and downward (~ 320 K – 340 K). The quasi-isentropic
281 transport occurs via two pathways (1) over Africa (20° E – 60° E) and (2) over the East Indian
282 Ocean and Western-Pacific (95° E – 140° E) (Fig. 4d-f). The downward penetration of
283 aerosols (BC, OC, and sulfate) in the Southern Hemisphere (15° S – 30° S) to 320 K – 340 K
284 via the above mentioned two pathways is also evident in Figure 4 g-i.

285 In the following, we further explore processes responsible for inter-hemispheric transport.
286 Our analysis indicates that the Hadley circulation (Fig. 5a and Fig. S3) with its ascending
287 branch over the Indian Ocean and adjoining region (60° E – 140° E, 0 – 30° N), lifts the South
288 Asian aerosols to the UTLS. These aerosols enter the westerly jet (Fig. 4 d-f).

289 The distribution of zonal winds in Fig. 5b shows transport into the southern hemisphere
290 preferentially in regions of equatorial westerly winds, so-called "westerly duct" regions
291 (Vaugh and Polvani, 2000; Yan et al., 2021), where Rossby-wave breaking occurs (Fig. 5b
292 and Fig. S4). This is consistent with findings from Frederiksen et al. (2018) who have also
293 shown interhemispheric transport of CO_2 via Pacific and Atlantic westerly ducts during the

294 spring season. Fig. 5c shows that changes in South Asian aerosols concentrations cause a
 295 shift in the Pacific duct. Thus interhemispheric transport occurs through (1) an Atlantic duct
 296 and (2) a slightly shifted Pacific duct ($5^{\circ} \text{S} - 5^{\circ} \text{N}$, $50^{\circ} \text{E} - 140^{\circ} \text{E}$), i.e. over the Indian-
 297 Ocean-Western Pacific region (also see Fig. 4 d-f). The shift in Pacific duct in a response to
 298 South Asian aerosol changes is likely due to higher Rossby wave bearing near south Asia.
 299 The geopotential (Fig 5d) and potential vorticity (Fig. S5) anomalies (CTL-Aerooff) show
 300 Rossby wave breaking near the Indian-Ocean-Western Pacific region that could lead to
 301 Southern hemispheric transport through the Indian-Ocean-Western Pacific region path (Fig 5
 302 c-d). In addition, the interhemispheric transport is also likely influenced by the monthly
 303 migration and the strength of the Hadley circulation (Fig. S3).



317 Figure 4: Meridional cross-section over Indian Ocean-western Pacific (averaged 30° E –
 318 140° E and for the spring season for the years 2001 – 2016) of anomalies (%) (CTL-
 319 Aerooff) of (a-c) BC, OC, and sulfate aerosols. Green contours in (a-c) indicate westerly jet.
 320 Fig (d-f) spatial distribution of BC, OC and Sulfate aerosols averaged at 360 – 390K
 321 isentropic levels and the spring season for the years 2001 – 2016, vectors in Figs. a-f
 322 indicate anomalies of winds (m s^{-1}). (g-h) Zonal cross-section (averaged over 15° S – 30° S
 323 and for the spring season for the years 2001 – 2016) and for the spring season for BC, OC,
 324 and sulfate aerosols. The black line of 2 PV in (a-c and g-i) indicates the dynamical
 325 tropopause.

326

327

328

329

330

331

332

333

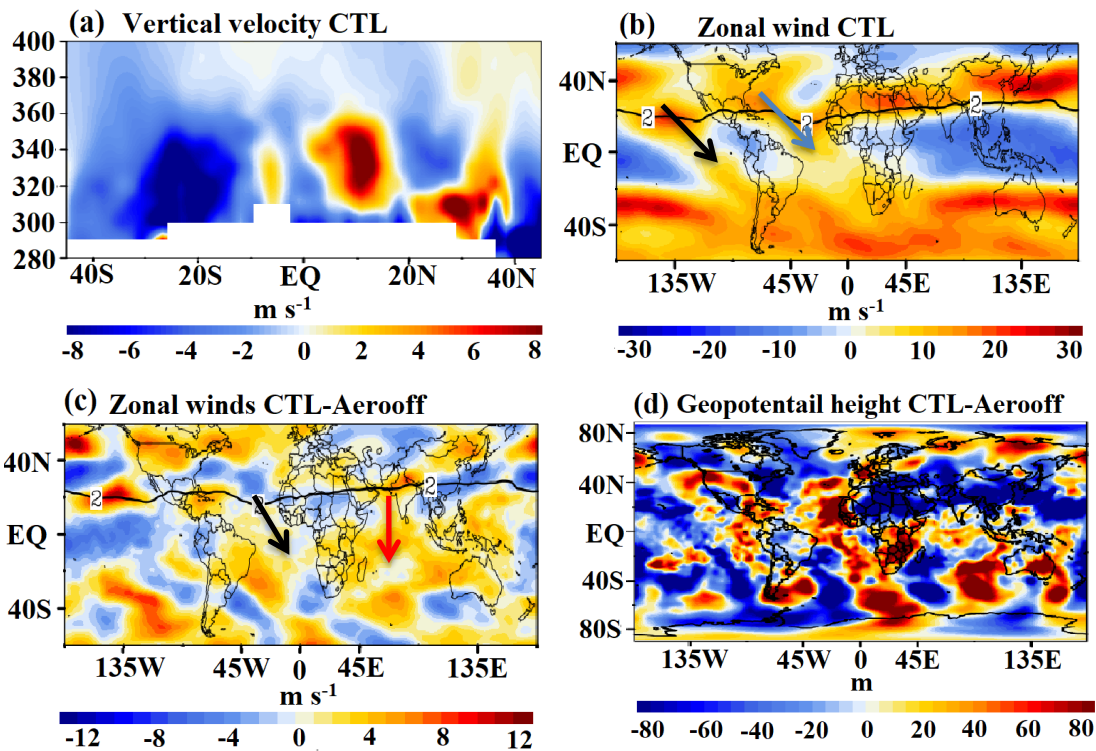
334

335

336

337

338



339 Figure 5: Meridional cross section of vertical velocities (m s^{-1}) (averaged for 65° E – 140° E
 340 and for spring season during 2001 – 2016). Vertical velocities are scaled by 300, (b) zonal
 341 winds at 360 K isentropic level from CTL simulations, a black arrow indicates Pacific duct
 342 and blue arrow indicates Atlantic duct, (c) anomalies (CTL-Aerooff) zonal winds at 360 K
 343 isentropic level. A black arrow indicates the Atlantic duct and red arrow indicates duct over
 344 the Indian Ocean, (d) anomalies (CTL-Aerooff) of geopotential height (m) at the 340K
 345 potential temperature level. The potential vorticity (2 PVU) is indicated by the black contour
 346 in Figs. a-c.

347

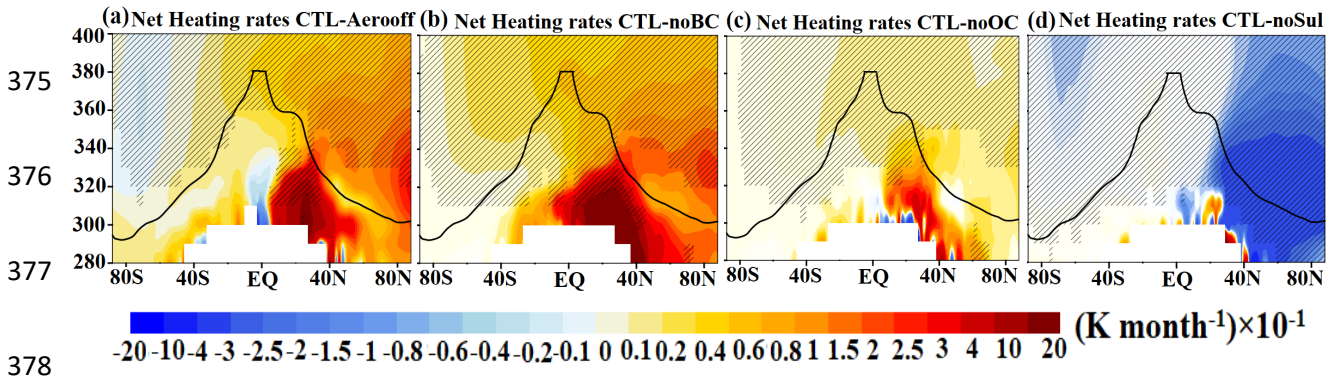
348 Further, in the UTLS, South Asian aerosols are transported to the Arctic (Fig. 4 a-c). There is
349 an aerosol enhancement in the Arctic (BC: 10 to 30 %, OC: 10 to 20 %, Sulfate: 5 to 30 %).
350 Our analysis shows that transport to the Arctic occurs every year in the UTLS which causes
351 heating in the lower stratosphere (380 K – 400K) (see Section 3.4).

352 **3.4. Impacts on the net heating rate and water vapour**

353 Carbonaceous aerosols absorb solar radiation, leading to atmospheric heating, while
354 predominately scattering aerosols such as sulfate reflect and scatter back solar radiation,
355 therefore cooling the atmosphere below (Fadnavis et al., 2019). Here, we analyse net heating
356 rates (short wave + long wave) induced by all the anthropogenic Asian aerosols (CTL -
357 Aerooff). Changes in the net heating rates are induced by the aerosol changes; any changes in
358 dynamical heating will be intrinsic. The vertical distribution of net heating rate anomalies
359 over the North Indian Ocean and Western Pacific region (30° E – 140° E) indicates increase
360 in heating rates in the region of elevated anthropogenic aerosols in the troposphere (0.15 to
361 0.4 K month⁻¹, 5 – 60 %) and UTLS (0.02 to 0.3 K month⁻¹, 10 – 60 %) (Fig. 6a-d, Fig. 4, and
362 Fig. S2). Heating rate anomalies estimated over the North Indian Ocean and western Pacific
363 region from BC (CTL - BCoff), OC (CTL - OCoff), and Sulfate (CTL - Suloff) show that BC
364 and OC aerosols produce heating in the troposphere (280K – 340K) (10° N – 40° N) (BC:
365 0.6 to 2 K month⁻¹, 10 – 50% , OC: 0.2 to 0.4 K month⁻¹, 0.5 – 4 %) and UTLS over Northern
366 hemisphere (BC: 0.08 to 0.2 K month⁻¹, 30 – 45%, OC: 0.02 to 0.06 K month⁻¹, 0.2 – 1.5 %),
367 while sulfate aerosols produce atmospheric cooling in the troposphere and UTLS -0.02 to -
368 0.4 K month⁻¹ (5 – 40 %) (280 - 400K) (Fig. 6a-d). Black carbon aerosol produces higher
369 heating than organic carbon aerosols. The shortwave heating due to BC aerosols is the major
370 contributor to the total heating. In general, these aerosols increase heating in the troposphere
371 extending to the lower stratosphere (400K) over the South Asian region (Fig. 6a). There is
372 enhancement in heating rates along the path of aerosols transported to the Arctic.

373

374



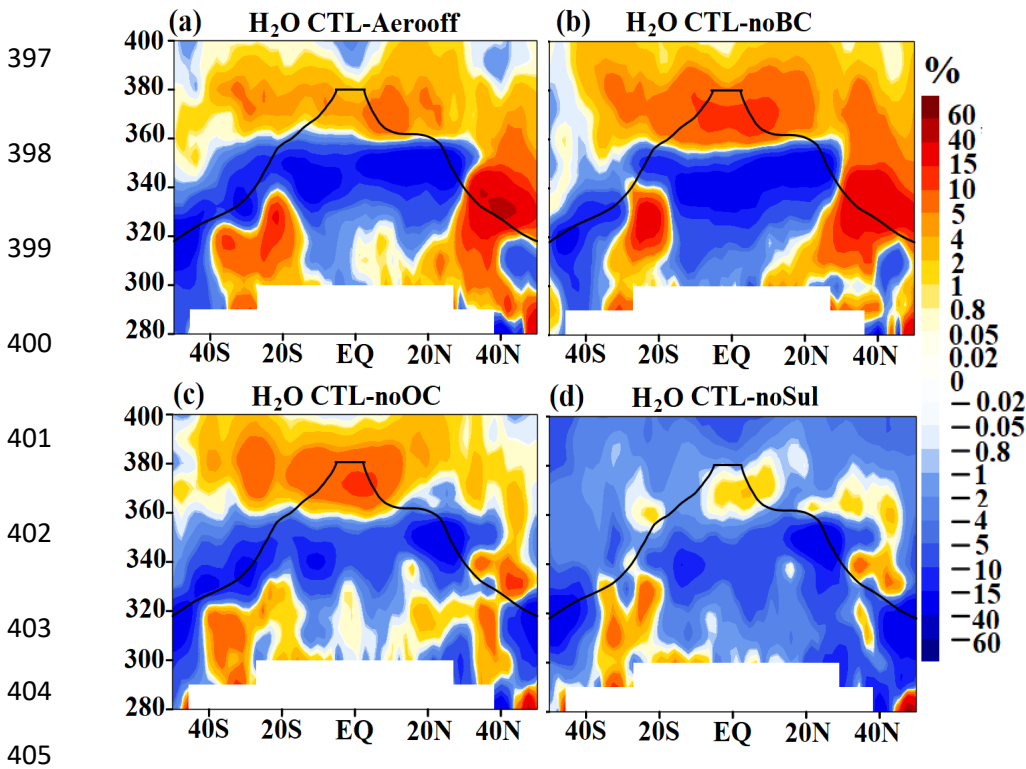
378

379 Figure 6: Meridional cross-section of heating rates (K month^{-1}) over the Indian Ocean-
380 western Pacific (averaged $30^\circ \text{ E} - 140^\circ \text{ E}$ and for the spring season for the years 2001 – 2016)
381 (a) from CTL - Aerooff simulation, (b) same (a) but from CTL - BCoff simulation (c) same
382 (a) but from CTL - OCoff simulation, (d) same (a) but from CTL - Suloff simulation. Hatches
383 in Figs. a-d indicate 95% significance level. A black line in Figs. a-d indicates the dynamical
384 tropopause.

385

386 The vertical distribution of water vapor over the Indian Ocean-Western Pacific region (30°
387 $\text{E} - 140^\circ \text{ E}$) (CTL - Aerooff) shows that water vapour concentrations are enhanced by 1-10%
388 along the path of elevated aerosols (Fig. 7a and Fig. 4). In the UTLS, water vapour is
389 transported to the southern hemisphere $\sim 45^\circ \text{ S}$. This may be due to heating caused by the
390 Asian aerosols. The impact of BC (CTL - BCoff), OC (CTL - OCoff), and Sulfate (CTL -
391 Suloff) on the water vapor distribution (Fig. 7 b-d) shows that BC aerosols play a major role
392 in water vapor enhancement in the UTLS (Fig. 7 b). Water vapor enhancement by BC
393 aerosols over the Indian Ocean-Western Pacific region is $\sim 1 - 15 \%$ (Fig. 7b). The water
394 vapor enhancement by OC aerosols in the UTLS region is $0.8 - 15\%$ (Fig. 7c) and by sulfate
395 aerosols $\sim 0.2 - 1\%$ in pockets (Fig. 7d).

396

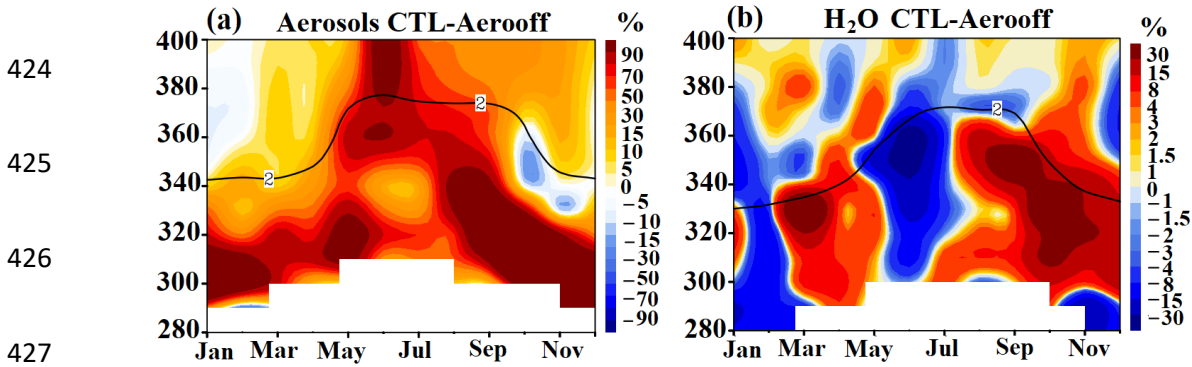


406 Figure 7: (a) Meridional cross-section over the Indian Ocean-western Pacific (averaged over
407 30° E – 140° E) of anomalies of water vapour (%) (CTL - Aerooff) the for spring season for
408 the years 2001 – 2016, (b) same as (a) but from CTL - BCoff simulations, (c) same as (a) but
409 from CTL - OCoff simulations, (d) same as (a) but from CTL - Suloff simulations. A black
410 line in Figs. a-d indicates the dynamical tropopause.

411

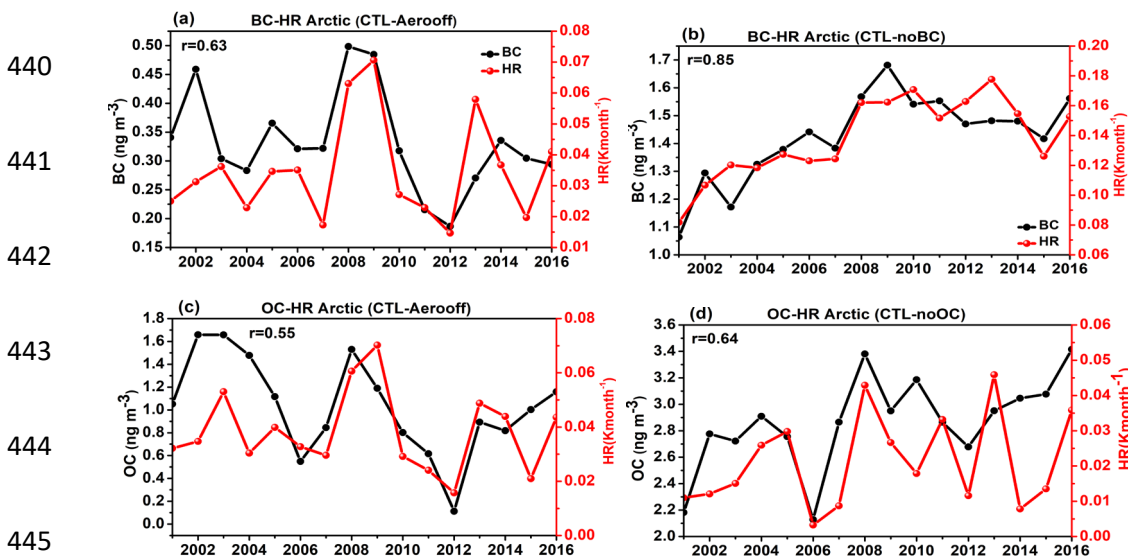
412 Although the focus of the manuscript is on the transport of aerosols during the spring season,
413 it should be noted that the anthropogenic South Asian aerosols are also transported to the
414 UTLS during the monsoon season (Shindell et al., 2008, Fadnavis et al., 2013, 2017, 2019,
415 Zheng et al., 2021). Annual distribution anomalies of aerosols (average of BC, OC, and
416 sulfate) show the transport of aerosols into the UTLS during the spring and monsoon seasons
417 (April to September) from South Asian region (Fig. 8a). In the lower stratosphere, these
418 aerosols persist for a few months (Fig. 8a) thus their effect will be seen for an extended time.
419 These aerosols enhance tropospheric heating thereby transporting elevated water vapour into
420 the lower stratosphere (Fig. 8b). Figure 8a also shows the transport of aerosols into the lower
421 stratosphere during spring and the monsoon seasons (March-September). The aerosol induced

422 enhanced water vapour also shows enhancement in the lower stratosphere during the same
 423 time (Fig. 8b).



428 Figure 8: (a) Annual distribution of anomalies of aerosols (CTL - Aerooff) (averaged of BC,
 429 OC and sulfate aerosols) (%) averaged South Asian region (50° E – 100° E, 20° N – 40° N),
 430 (b) same as (a) but for water vapour (%) over North Indian-Ocean-Western-Pacific (30° E –
 431 140° E, 20° N – 40° N). A black line in Figs. a-b indicates the dynamical tropopause.

432 Further, we analyze the correlation between heating rates and carbonaceous aerosol
 433 amounts in the UTLS (380 K level) in the Arctic during 2001 – 2016 (spring mean) (Fig. 9)
 434 from Aerooff, BCoff, and OCOff in comparison with CTL simulations. The carbonaceous
 435 aerosols show a positive correlation (correlation coefficient r : 0.55 to 0.85) with the UTLS
 436 heating rates indicating that transported carbonaceous aerosols enhance UTLS heating in the
 437 Arctic. It should be noted that increase in aerosols at the Arctic also occurs during the
 438 monsoon season (Fadnavis et al., 2017a, 2017b, 2019, Zheng et al., 2021) which may affect
 439 the dynamics and aerosol amounts in the spring of the next year in the UTLS.



446 Figure 9: (a) Time series of BC aerosols and heating rates averaged for spring in the UTLS
447 (380 K) in the Arctic (65° N – 85° N, 0 – 360°) (from CTL – Aerooff), (b) same as (a) but
448 from CTL – BCoff. (c) same as (a) but for OC, (d) same as (c) but form CTL – OCoff. The
449 correlation coefficient (r) between anomalies of BC/OC aerosols and heating rates is
450 indicated in panels a-d.

451

452 Importantly, South Asian aerosols enhance water vapor in the lower stratosphere in the
453 tropical and subtropical latitudes (45° S – 45° N). Water vapor being a greenhouse gas further
454 enhances the heating of the troposphere leading to a positive feedback. The increase in water
455 vapor in the stratosphere also warms the Earth's surface (Shindell, 2001; Solomon et al.,
456 2010). Solomon et al. (2010) estimated that an increase in the stratospheric water vapor by 1
457 ppmv accounts for 0.24 W m⁻² radiative forcing at the TOA. The SABER and MLS
458 observations showed an increase in stratospheric water vapor by 0.45 ppmv globally during
459 2003 – 2017 (Yue et al., 2019). Thus the radiative forcing due to water vapor increase (0.02 –
460 0.14 ppmv) in response to South Asian anthropogenic aerosols is not negligible for surface
461 warming globally. Further, increasing stratospheric water vapour could also lead to ozone
462 depletion (e.g., Shindell, 2001, Robrecht et al., 2019).

463 **4. Conclusions**

464 A series of ECHAM6-HAMMOZ chemistry-climate simulations for South Asian
465 anthropogenic aerosols were used to understand the transport pathways of South Asian
466 aerosols in spring and their impacts on the UTLS. The model simulations show that large
467 amounts of South Asian aerosols are transported during spring to the Arabian Sea (increases
468 in AOD by: 0.02 – 0.12 from CTL - Aerooff) and Bay of Bengal (increases in AOD by: 0.16
469 to 0.8 from CTL - Aerooff) and Western Pacific (increases in AOD by 0.08 to 0.18). These
470 aerosols are further lifted up into the UTLS from the North Indian Ocean and South Asia (10°
471 N – 30° N). In the UTLS, they are also transported to the southern hemisphere (15° S – 30°

472 S) and downward (320K – 340K). The processes responsible for interhemispheric transport
473 are as follows:

474 (1) South Asian aerosols are lifted up to the UTLS by the ascending branch of Hadley
475 circulation. In the UTLS the aerosols enter the westerly Jet.

476 (2) They are transported to the Southern hemisphere via the Atlantic westerly duct (5° S – 5°
477 N, 10° W – 40° W) and Pacific westerly duct (5° S – 5° N, 50° E – 140° E),

478 (3) A shift in the Pacific westerly duct may be due to an increase in Rossby Wave Breaking
479 over the north Indian Ocean-western Pacific induced by South Asian aerosols.

480 The anthropogenic aerosol produces significant radiative impacts over the Indo-Gangetic
481 Plain (RF anomalies estimated from CTL-Aerooff simulations, TOA: $+1.27 \pm 0.16 \text{ W m}^{-2}$,
482 Surface: $-11.16 \pm 0.50 \text{ W m}^{-2}$, In-atmosphere: $+12.44 \pm 0.42 \text{ W m}^{-2}$) and the Arabian Sea (RF at
483 the TOA: $-0.72 \pm 0.14 \text{ W m}^{-2}$, surface: $-3.00 \pm 0.28 \text{ W m}^{-2}$, In-atmosphere: $+2.27 \pm 0.19 \text{ W m}^{-2}$).
484 Interestingly, RF at the TOA over the Indo-Gangetic Plain is positive ($+4.33 \pm 0.17 \text{ W m}^{-2}$)
485 due to the emission of BC aerosols alone. The anthropogenic aerosols enhance heating in the
486 troposphere over the North Indian Ocean (estimated from CTL-Aerooff) by 0.15 to 0.4 K
487 month⁻¹ (4 – 60 %) and UTLS by 0.02 to 0.3 K month⁻¹ (10 – 60 %).

488 The heating of the troposphere by the carbonaceous aerosol (mainly BC) increases
489 temperature and thereby tropospheric water vapor amounts over the North Indian Ocean and
490 adjoining regions. The elevated water vapor is transported to the UTLS from the North Indian
491 ocean-western Pacific region (30° E – 140° E, 20° N – 40° N). In the UTLS it is transported
492 to the Southern Hemisphere ~45° S. BC aerosols play a major role in water vapor
493 enhancement in the lower stratosphere (increased water vapor by 0.8 – 5 %). As water vapour
494 is a greenhouse gas, this enhancement of stratospheric water vapour could potentially amplify

495 the warming of the troposphere and surface and cause a positive feedback (e.g. Shindell,
496 2001; Solomon et al., 2010).

497 *Acknowledgments:* The authors thank the staff of the High Power Computing Centre (HPC)
498 in the Indian Institute of Tropical Meteorology, Pune, India, Pune, India. We thank the
499 reviewers for their valuable suggestions. We thank Jonathon Wright for useful discussions
500 and suggestions that improved the quality of the manuscript.

501 **Data availability:** The data used in this study are generated from ECHAM6-HAMMOZ
502 model simulations at the High-performance computing system in the Indian Institute of
503 Tropical Meteorology, Pune, India. The AOD data from MODIS Terra used here can be
504 downloaded from <https://ladsweb.modaps.eosdis.nasa.gov/archive/allData/61/MODATML2/>,
505 and MISR from <https://misr.jpl.nasa.gov/getData/accessData/>.

506

507 **Author contributions:** S. F. initiated the idea. A. J., S. S., A. A., performed model analysis.
508 R. M., and A. R. contributed to analysis and study design. All authors contributed to the
509 writing and discussions of the manuscript.

510

511 **Competing Interests:** Some authors are members of the editorial board of Atmospheric
512 Chemistry and Physics. The peer-review process was guided by an independent editor, and
513 the authors have also no other competing interests to declare.

514

515 **References:**

- 516 Aswini, A. R., Hegde, P., Aryasree, S., Girach, I. A. and Nair, P. R.: Continental outflow of
517 anthropogenic aerosols over Arabian Sea and Indian Ocean during wintertime: ICARB-
518 2018 campaign, *Sci. Total Environ.*, 712, 135214, doi:10.1016/j.scitotenv.2019.135214,
519 2020.
- 520 Babu, S. S., Manoj, M. R., Moorthy, K. K., Gogoi, M. M., Nair, V. S., Kompalli, S. K.,
521 Satheesh, S. K., Niranjana, K., Ramagopal, K., Bhuyan, P. K. and Singh, D.: Trends in
522 aerosol optical depth over Indian region: Potential causes and impact indicators, *J.*
523 *Geophys. Res. Atmos.*, 118, 11,794-11,806, doi:10.1002/2013JD020507, 2013.
- 524 Budhavant, K., Bikkina, S., Andersson, A., Asmi, E., Backman, J., Kesti, J., Zahid, H.,
525 Satheesh, S. K. and Gustafsson, Ö.: Anthropogenic fine aerosols dominate the
526 wintertime regime over the northern Indian Ocean, *Tellus, Ser. B Chem. Phys.*
527 *Meteorol.*, 70, 1–15, doi:10.1080/16000889.2018.1464871, 2018.
- 528 Chavan, P., Fadnavis, S., Chakroborty, T., Sioris, C. E. and Müller, R.: The outflow of Asian
529 biomass burning carbonaceous aerosol into the UTLS in spring: Radiative effects seen
530 in a global model, 21, 14371–14384, <https://doi.org/10.5194/acp-2021-494>, 2021.
- 531 Corrigan, C. E., Roberts, G. C., Ramana, M. V., Kim, D. and Ramanathan, V.: Capturing
532 vertical profiles of aerosols and black carbon over the Indian Ocean using autonomous
533 unmanned aerial vehicles, *Atmos. Chem. Phys.*, 8, 737–747, doi:10.5194/acp-8-737-
534 2008, 2008.
- 535 Collins, M., Sutherland, M., Bouwer, L., Cheong, S.-M., Frölicher, T. L., Jacot Des Combes,
536 H., Roxy, M. K., Losada, I., McInnes, K. L., Ratter, B., Rivera-Arriaga, E., Susanto, R.
537 D., Swingedouw, D., Tibig, L., Bakker, P., Eakin, C. M., Emanuel, K., Grose, M.,
538 Hemer, M., Jackson, L., Kääh, A., Kajtar, J. B., Knutson, T., Laufkötter, C., Noy, I.,

539 Payne, M., Ranasinghe, R., Sgubin, G. and Timmermans, M.-L.: Extremes, Abrupt
540 Changes and Managing Risks, IPCC Spec. Rep. Ocean Cryosph. a Chang. Clim., 589–
541 655, 2019.

542 De Reus, M., Krejci, R., Williams, J., Fischer, H., Scheele, R. and Ström, J.: Vertical and
543 horizontal distributions of the aerosol number concentration and size distribution over
544 the northern Indian Ocean, *J. Geophys. Res. Atmos.*, 106, 28629–28641,
545 doi:10.1029/2001JD900017, 2001.

546 Dickerson, R. R., Andreae, M. O., Campos, T., Mayol-Bracero, O. L., Neusuess, C. and
547 Streets, D. G.: Analysis of black carbon and carbon monoxide observed over the Indian
548 Ocean: Implications for emissions and photochemistry, *J. Geophys. Res. Atmos.*, 107,
549 doi:10.1029/2001JD000501, 2002.

550 Fadnavis, S., Kalita, G., Rowlinson, M., Rap, A., Li, J.-L. F., Gasparini, B., Laakso, A. and
551 Müller, R.: The impact of increases in South Asian anthropogenic emissions of SO₂ on
552 sulfate loading in the upper troposphere and lower stratosphere during the monsoon
553 season and the associated radiative changes, *Atmos. Chem. Phys.*, 19, 9989–10008,
554 <https://doi.org/10.5194/acp-19-9989-2019>, 2019.

555 Fadnavis, S., Roy, C., Sabin, T. P., Ayantika, D. C. and Ashok, K.: Potential modulations of
556 pre-monsoon aerosols during El Niño: impact on Indian summer monsoon, *Clim. Dyn.*,
557 49, 2279–2290, doi:10.1007/s00382-016-3451-6, 2017a.

558 Fadnavis, S., Kalita, G., Ravi Kumar, K., Gasparini, B. and Li, J. L. F.: Potential impact of
559 carbonaceous aerosol on the upper troposphere and lower stratosphere (UTLS) and
560 precipitation during Asian summer monsoon in a global model simulation, *Atmos.*
561 *Chem. Phys.*, 17, 11637–11654, doi:10.5194/acp-17-11637-2017, 2017b.

562 Fadnavis, S. and Chattopadhyay, R.: Linkages of subtropical stratospheric intraseasonal

563 intrusions with Indian summer monsoon deficit rainfall, *J. Clim.*, 30, 5083–5095,
564 doi:10.1175/JCLI-D-16-0463.1, 2017.

565 Fadnavis, S., Semeniuk, K., Pozzoli, L., Schultz, M. G., Ghude, S. D., Das, S. and Kakatkar,
566 R.: Transport of aerosols into the UTLS and their impact on the asian monsoon region
567 as seen in a global model simulation, *Atmos. Chem. Phys.*, 13, 8771–8786,
568 doi:10.5194/acp-13-8771-2013, 2013.

569 Fadnavis, S., Sabin, T. P., Rap, A., Müller, R., Kubin, A. and Heinold, B.: The impact of
570 COVID-19 lockdown measures on the Indian summer monsoon, *Environ. Res. Lett.*,
571 16, 074054, doi:10.1088/1748-9326/ac109c, 2021a.

572 Fadnavis S., Müller R , Chakraborty T. , Sabin T. P., Laakso A. , Rap A. , Griessbach S.,
573 Vernier J-P., and Tilmes S., The role of tropical volcanic eruptions in exacerbating
574 Indian droughts, *Sci. Rep.*, 11, 2714, doi.org/10.1038/s41598-021-81566-0, 2021b.

575 Frederiksen, J. S. and Francey, R. J.: Unprecedented strength of Hadley circulation in 2015–
576 2016 impactson CO2 interhemispheric difference, *Atmos. Chem. Phys.*, 18, 14837–
577 14850, <https://doi.org/10.5194/acp-18-14837-2018>, 2018.

578 [Holton, J. R., Haynes, P. H., McIntyre, M. E., Douglass, A. R., Rood, R. B., Pfister, L.:](#)
579 [Stratosphere-troposphere exchange, *Reviews of Geophysics*, 33, 403-439,](#)
580 <https://doi.org/10.1029/95RG02097>, 1995.

581 Jose, S., Nair, V. S. and Babu, S. S.: Anthropogenic emissions from South Asia reverses the
582 aerosol indirect effect over the northern Indian Ocean, *Sci. Rep.*, 10, 18360,
583 doi:10.1038/s41598-020-74897-x, 2020.

584 Karambelas, A., Holloway, T., Kinney, P. L., Fiore, A. M., Defries, R., Kieseewetter, G. and
585 Heyes, C.: Urban versus rural health impacts attributable to PM2.5 and O₃ in northern
586 India, *Environ. Res. Lett.*, 13, 064010, doi:10.1088/1748-9326/aac24d, 2018.

587 Kahn, R. A., Garay, M. J., Nelson, D. L., Yau, K. K., Bull, M. A., Gaitley, B. J., Martonchik,
588 J. V., and Levy, R. C.: Satellite-derived aerosol optical depth over dark water from
589 MISR and MODIS: Comparisons with AERONET and implications for climatological
590 studies, *J. Geophys. Res.*, 112, D18205, doi:10.1029/2006JD008175, 2007.

591 Kunz, A., Konopka, P., Müller, R. and Pan, L. L.: The dynamical tropopause based on
592 isentropic potential vorticity gradients *J. Geophys. Res.*, 116, D01110,
593 doi:10.1029/2010JD014343, 2011.

594 Lu, Z., Zhang, Q. and Streets, D. G.: Sulfur dioxide and primary carbonaceous aerosol
595 emissions in China and India, 1996-2010, *Atmos. Chem. Phys.*, 11, 9839–9864,
596 doi:10.5194/acp-11-9839-2011, 2011.

597 Mahowald, N. M., Hamilton, D. S., Mackey, K. R. M., Moore, J. K., Baker, A. R., Scanza, R.
598 A. and Zhang, Y.: Aerosol trace metal leaching and impacts on marine microorganisms,
599 *Nat. Commun.*, 9, 2614, doi:10.1038/s41467-018-04970-7, 2018.

600 Mayol-Bracero, O. L., Gabriel, R., Andreae, M. O., Kirchstetter, T. W., Novakov, T., Ogren,
601 J., Sheridan, P. and Streets, D. G.: Carbonaceous aerosols over the Indian Ocean during
602 the Indian Ocean Experiment (INDOEX): Chemical characterization, optical properties,
603 and probable sources, *J. Geophys. Res. Atmos.*, 107, 8030,
604 doi:10.1029/2000JD000039, 2002.

605 McFarquhar, G. M. and Wang, H.: Effects of aerosols on trade wind cumuli over the Indian
606 Ocean: Model simulations, *Q. J. R. Meteorol. Soc.*, 132, 821–843,
607 doi:10.1256/qj.04.179, 2006.

608 Meehl, G. A., Arblaster, J. M. and Collins, W. D.: Effects of black carbon aerosols on the
609 Indian monsoon, *J. Clim.*, 21, 2869–2882, doi:10.1175/2007JCLI1777.1, 2008.

610 Nair, V. S., Babu, S. S., Manoj, M. R., Moorthy, K. K. and Chin, M.: Direct radiative effects
611 of aerosols over South Asia from observations and modeling, *Clim. Dyn.*, 49, 1411–
612 1428, doi:10.1007/s00382-016-3384-0, 2017.

613 Neubauer, D., Lohmann, U., Hoose, C. and Frontoso, M. G.: Impact of the representation of
614 marine stratocumulus clouds on the anthropogenic aerosol effect, *Atmos. Chem. Phys.*,
615 14, 11997–12022, doi:10.5194/acp-14-11997-2014, 2014.

616 Paliwal, U., Sharma, M. and Burkhart, J. F.: Monthly and spatially resolved black carbon
617 emission inventory of India: Uncertainty analysis, *Atmos. Chem. Phys.*, 16, 12457–
618 12476, doi:10.5194/acp-16-12457-2016, 2016.

619 Papaspiropoulos, G., Martinsson, B. G., Zahn, A., Brenninkmeijer, C. A. M., Hermann, M.,
620 Heintzenberg, J., Fischer, H. and Van Velthoven, P. F. J.: Aerosol elemental
621 concentrations in the tropopause region from intercontinental flights with the Civil
622 Aircraft for Regular Investigation of the Atmosphere Based on an Instrument Container
623 (CARIBIC) platform, *J. Geophys. Res. Atmos.*, 107, 4671, doi:10.1029/2002JD002344,
624 2002.

625 Pathak, H. S., Satheesh, S. K., Moorthy, K. K. and Nanjundiah, R. S.: Assessment of regional
626 aerosol radiative effects under the SWAAMI campaign - Part 2: Clear-sky direct
627 shortwave radiative forcing using multi-year assimilated data over the Indian
628 subcontinent, *Atmos. Chem. Phys.*, 20, 14237–14252, doi:10.5194/acp-20-14237-2020,
629 2020.

630 Penner, J. E., Chuang, C. C. and Grant, K.: Climate forcing by carbonaceous and sulfate
631 aerosols, *Clim. Dyn.*, 14, 839–851, doi:10.1007/s003820050259, 1998.

632 Ploeger, F., Konopka, P., Walker, K., and Riese, M.: Quantifying pollution transport from the
633 Asian monsoon anticyclone into the lower stratosphere, *Atmos. Chem. Phys.*, 17, 7055–

634 7066, <https://doi.org/10.5194/acp-17-7055-2017>, 2017.

635 Rajeev, K. and Ramanathan, V.: Direct observations of clear-sky aerosol radiative forcing
636 from space during the Indian Ocean Experiment, *J. Geophys. Res. Atmos.*, 106, 17221–
637 17235, doi:10.1029/2000JD900723, 2001.

638 Ramachandran, S., Rupakheti, M. and Lawrence, M. G.: Aerosol-induced atmospheric
639 heating rate decreases over South and East Asia as a result of changing content and
640 composition, *Sci. Rep.*, 10, 20091, doi:10.1038/s41598-020-76936-z, 2020a.

641 Ramachandran, S., Rupakheti, M. and Lawrence, M. G.: Black carbon dominates the aerosol
642 absorption over the Indo-Gangetic Plain and the Himalayan foothills, *Environ. Int.*,
643 142, 105814, doi:10.1016/j.envint.2020.105814, 2020b.

644 Ramanathan, V., Chung, C., Kim, D., Bettge, T., Buja, L., Kiehl, J. T., Washington, W. M.,
645 Fu, Q., Sikka, D. R. and Wild, M.: Atmospheric brown clouds: Impacts on South Asian
646 climate and hydrological cycle, *Proc. Natl. Acad. Sci. U. S. A.*, 102, 5326–5333,
647 doi:10.1073/pnas.0500656102, 2005.

648 Ramanathan, V., Crutzen, P. J., Lelieveld, J., Mitra, A. P., Althausen, D., Anderson, J.,
649 Andreae, M. O., Cantrell, W., Cass, G. R., Chung, C. E., Clarke, A. D., Coakley, J. A.,
650 Collins, W. D., Conant, W. C., Dulac, F., Heintzenberg, J., Heymsfield, A. J., Holben,
651 B., Howell, S., Hudson, J., Jayaraman, A., Kiehl, J. T., Krishnamurti, T. N., Lubin, D.,
652 McFarquhar, G., Novakov, T., Ogren, J. A., Podgorny, I. A., Prather, K., Priestley, K.,
653 Prospero, J. M., Quinn, P. K., Rajeev, K., Rasch, P., Rupert, S., Sadourny, R., Satheesh,
654 S. K., Shaw, G. E., Sheridan, P. and Valero, F. P. J.: Indian Ocean Experiment: An
655 integrated analysis of the climate forcing and effects of the great Indo-Asian haze, *J.*
656 *Geophys. Res. Atmos.*, 106, 28371–28398, doi:10.1029/2001JD900133, 2001.

657 Robrecht, S., Vogel, B., Grooß, J.-U., Rosenlof, K., Thornberry, T., Rollins, A., Krämer, M.,

658 Christensen, L. and Müller, R.: Mechanism of ozone loss under enhanced water vapour
659 conditions in the mid-latitude lower stratosphere in summer, *Atmos. Chem. Phys.*, 19,
660 5805–5833, doi:10.5194/acp-19-5805-2019, 2019.

661 Romatschke, U. and Houze, R. A.: Characteristics of precipitating convective systems in the
662 South Asian monsoon, *J. Hydrometeorol.*, 12, 3–26, doi:10.1175/2010JHM1289.1,
663 2011.

664 Satheesh, S. K., Ramanathan, V., Holben, B. N., Krishna Moorthy, K., Loeb, N. G., Mating,
665 H., Prospero, J. M. and Savoie, D.: Chemical, microphysical, and radiative effects of
666 Indian Ocean aerosols, *J. Geophys. Res.*, 107, 4725, doi:10.1029/2002JD002463, 2002.

667 Satheesh, S. K. and Ramanathan, V.: Large differences in tropical aerosol forcing at the top
668 of the atmosphere and Earth’s surface, *Nature*, 405, 60–63, doi:10.1038/35011039,
669 2000.

670 Shindell, D. T.: Climate and ozone response to increased stratospheric water vapor, *Geophys.*
671 *Res. Lett.*, 28, 1551–1554, doi:10.1029/1999GL011197, 2001.

672 Solomon, S., Rosenlof, K. H., Portmann, R. W., Daniel, J. S., Davis, S. M., Sanford, T. J. and
673 Plattner G. K.: Contributions of stratospheric water vapor to decadal changes in the rate
674 of global warming, *Science*, 327, 1219–1223, 0.1126/science.1182488, 2010.

675 Shindell, D. T., Chin, M., Dentener, F., Doherty, R. M., Faluvegi, G., Fiore, A. M., Hess, P.,
676 Koch, D. M., MacKenzie, I. A., Sanderson, M. G., Schultz, M. G., Schulz, M.,
677 Stevenson, D. S., Teich, H., Textor, C., Wild, O., Bergmann, D. J., Bey, I., Bian, H.,
678 Cuvelier, C., Duncan, B. N., Folberth, G., Horowitz, L. W., Jonson, J., Kaminski, J. W.,
679 Marmer, E., Park, R., Pringle, K. J., Schroeder, S., Szopa, S., Takemura, T., Zeng, G.,
680 Keating, T. J., and Zuber, A.: A multi-model assessment of pollution transport to the

681 [Arctic, Atmos. Chem. Phys., 8, 5353–5372, https://doi.org/10.5194/acp-8-5353-2008,](https://doi.org/10.5194/acp-8-5353-2008)
682 [2008.](https://doi.org/10.5194/acp-8-5353-2008)

683 Stier, P., Feichter, J., Kinne, S., Kloster, S., Vignati, E., Wilson, J., Ganzeveld, L., Tegen, I.,
684 Werner, M., Balkanski, Y., Schulz, M., Boucher, O., Minikin, A., and Petzold, A.: The
685 aerosol-climate model ECHAM5-HAM, *Atmos. Chem. Phys.*, 5, 1125–1156,
686 doi:10.5194/acp-5-1125-2005, 2005.

687 Taylor, K. E., Williamson, D. L. and Zwiers, F. W.: The Sea Surface Temperature and Sea-
688 Ice Concentration Boundary Conditions for AMIP II Simulations, Program for Climate
689 Model Diagnosis and Intercomparison (PCMDI), Lawrence Livermore Natl. Lab.
690 Livermore, Calif., Rep., 60, 1–28 <http://www-pcmdi.llnl.gov/publications/ab60.html>,
691 2000.

692 Tegen, I., Neubauer, D., Ferrachat, S., Drian, C. S. Le, Bey, I., Schutgens, N., Stier, P.,
693 Watson-Parris, D., Stanelle, T., Schmidt, H., Rast, S., Kokkola, H., Schultz, M.,
694 Schroeder, S., Daskalakis, N., Barthel, S., Heinold, B. and Lohmann, U.: The global
695 aerosol-climate model echam6.3-ham2.3 -Part 1: Aerosol evaluation, *Geosci. Model*
696 *Dev.*, 12, 1643–1677, doi:10.5194/gmd-12-1643-2019, 2019.

697 Tegen, I., Harrison, S. P., Kohfeld, K. E., Prentice, I. C., Coe, M., and Heimann, M.: Impact
698 of vegetation and preferential source areas on global dust aerosol: Results from a model
699 study, *J. Geophys. Res.-Atmos.*, 107, 14–27, <https://doi.org/10.1029/2001JD000963>,
700 2002.

701 Waugh, D. W. and Polvani, L. M.: Intrusions into the tropical upper troposphere, *Geophys.*
702 *Res. Lett.*, 27, 3857–3860, <https://doi.org/10.1029/2000GL012250>, 2000.

703 [Yan, X., Konopka, P., Hauck, M., Podglajen, A., and Ploeger, F.: Asymmetry and pathways](#)

704 of inter-hemispheric transport in the upper troposphere and lower stratosphere, *Atmos.*
705 *Chem. Phys.*, 21, 6627–6645, <https://doi.org/10.5194/acp-21-6627-2021>, 2021.

706 Yue, J., Russell, J., Gan, Q., Wang, T., Rong, P., Garcia, R. and Mlynczak, M.: Increasing
707 Water Vapor in the Stratosphere and Mesosphere After 2002, *Geophys. Res. Lett.*, 46,
708 13452–13460, doi:10.1029/2019GL084973, 2019.

709 Zhang, K., O'Donnell, D., Kazil, J., Stier, P., Kinne, S., Lohmann, U., Ferrachat, S., Croft,
710 B., Quaas, J., Wan, H., Rast, S. and Feichter, J.: The global aerosol-climate model
711 ECHAM-HAM, version 2: Sensitivity to improvements in process representations,
712 *Atmos. Chem. Phys.*, 12, 8911–8949, doi:10.5194/acp-12-8911-2012, 2012.

713 Zheng, C., Wu, Y., Ting, M., Orbe, C., Wang, X., and Tilmes, S.: Summertime transport
714 pathways from different northern hemisphere regions into the Arctic. *Journal of*
715 *Geophysical Research: Atmospheres*, 126, e2020JD033811. [https://doi.](https://doi.org/10.1029/2020JD033811)
716 [org/10.1029/2020JD033811](https://doi.org/10.1029/2020JD033811), 2021